A NEW WAY OF THINKING ABOUT IMPACT MONITORING OF NEAR-EARTH OBJECTS

G. Tommei

Department of Mathematics, University of Pisa, Pisa, Italy, Email: giacomo.tommei@unipi.it

ABSTRACT

An asteroid just been discovered has a strongly undetermined orbit, being weakly constrained by the few available astrometric observations, and there is a set of possible orbits, all compatible with the observations, forming a Confidence Region (CR) in the 6-dimensional orbital elements space. The goal of Impact Monitoring (IM) is to understand whether the CR contains subsets of initial conditions leading to a collision with the Earth in the future (Virtual Impactors, VIs) and to estimate the Impact Probability (IP). Once defined the CR, the crucial steps are the sampling of the uncertainty region, the propagation of the so called Virtual Asteroids (VAs) searching for VIs and the computation of IP. Two automatic systems, CLOMON2 (at University of Pisa/SpaceDyS/ESA-NEOCC) and Sentry (at JPL/NASA), have been developed for this purpose. Both generate VAs by applying a 1-dimensional sampling of the CR based upon the Line Of Variations (LOV), that is a differentiable curve representing a kind of spine of the uncertainty region. The LOV method is very useful when the CR is elongated and thin, but this is not the case when the observed arc is very short: the uncertainty results to be wide in at least two directions and the LOV is not a reliable representative of the entire region. Unfortunately, this is precisely the case of very small asteroids observed only shortly before a close approach or an impact with the Earth (imminent impactors). The problem has been faced recently and three systems were developed, SCOUT (at JPL/NASA), NEORANGER (at University of Helsinki) and NEOScan (at University of Pisa/SpaceDyS): we will focus on the latter. NEOScan consults the NEO Confirmation Page (NEOCP) of the Minor Planet Center (MPC) every two minutes, extracting data and running the algorithms based on the Admissible Region (AR), a tool widely used also in the space debris orbit determination. Once an object goes away from the NEOCP obtaining a designation, the IM systems switch to "classical" 1-d algorithms. In this procedure, essentially dictated by the rules of the MPC, there is a flaw, in the sense that there are objects, with a very well-defined orbit, remaining on the NEOCP, and, on the contrary, there exist designated objects with a great uncertainty. Thus, there are a certain number of cases that are not properly processed. In this paper, after a review of the IM algorithms developed at the University of Pisa, we will present the idea of a new automatic system capable, starting from the astrometric observations, to decide what is the right algorithm in order to reach reasonable results for each kind of orbit.

Keywords: Near-Earth Objects; Impact Monitoring; Imminent Impactors; Astrometry; Line Of Variation; Manifold Of Variation.

1. INTRODUCTION

Every night professional and amateur astronomers observe the sky searching for new natural objects (asteroids, comets) or already discovered objects. The observations collected are sent to the Minor Planet Center (MPC), that, under the auspices of the International Astronomical Union (IAU), computes orbits and try to define the type of object. New discoveries that could be NEAs (Near-Earth Asteroids) are posted by the MPC on the NEO confirmation page (NEOCP, [6]). Once additional observations are collected and an orbit calculated, the object is added to the catalog of known objects, and such data are released through a Minor Planet Electronic Circular (MPEC). The discovery of a NEA is a process requiring the distinction between known and unknown objects, and then following up (obtaining additional observations) any unknown targets with the aim of extending the arc of observations and determining the orbit ([20]). Once an asteroid is discovered, it is important to clarify if it represents a risk for the Earth in a near or remote future: this is the goal of Impact Monitoring (IM), a relative young field of research. Since a significant amount of new observations are submitted every day, this activity requires an automatic system scanning continually the NEA catalog. This requirement has been achieved by CLOMON2 and Sentry, two independent IM systems that are operational at the University of Pisa/SpaceDyS/NEOCC (since 1999) and at NASA Jet Propulsion Laboratory (since 2002), respectively. During the time span over which observations are collected, CLOMON2 and Sentry outcomes ([9]), eventually with the announcement that some asteroid has the possibility of impacting, are published on the web: CLOMON2 results are published in the on-line information system NEODyS (*newton.spacedys.con/neodys*) and in the ESA portal (*neo.ssa.esa.int*), while Sentry re-

sults are available at CNEOS (*cneos.jpl.nasa.gov/sentry*). These two systems, whose output is carefully compared, now guarantee that the potentially dangerous objects are identified very early and followed up. The input data comes from the MPEC, thus an object is processed once is a confirmed NEO. Unfortunately there is the possibility that a small object discovered and listed on the NEOCP would strike the Earth in a near future. These objects are called *imminent impactors* and deserve a different treatment. For this reason, new mathematical algorithms and three automatic systems were developed recently, SCOUT (at JPL/NASA, [4]), NEORANGER (at University of Helsinki, [13]) and NEOScan (at University of Pisa/SpaceDyS, [14]).

In this paper, after a brief review of IM tools and techniques (Section 2), we will focus on the problem of imminent impactors describing the algorithms implemented in NEOScan and showing how it worked in a real case (Section 3). In Section 4 we will explore some possible future developments and the idea of building an unique automatic system capable of treat both imminent impactors and classical IM cases.

2. IMPACT MONITORING OVERVIEW

Impact Monitoring (IM) is the set of mathematical tools and techniques used to study the possibility of impact of an asteroid/comet with our planet. The output of an IM algorithm is a Virtual Impactor (VI) representative, that is an explicit set of initial conditions compatible with observations and leading to a collision at a given date. The main goal of IM is to solicit astrometric follow-up to either confirm or more likely dismiss the announced risk cases: this is achieved by communicating the impact date, the impact probability and the estimated impact energy. The steps of an IM procedure are the following.

1. **Acquisition of astrometrical data.** The observational data are acquired through the MPEC or scanning the NEOCP.

2. **Orbit Determination (OD).** Starting from the astrometry, it is possible to compute a preliminary orbit, using for example classical methods like the Gauss' one ([11]). Then a weighted Least Squares (LS) method has to be performed searching for a minimum $\mathbf{x}^*$ of the *target function*

$$Q(\mathbf{x}) = \frac{1}{m}\,\xi(\mathbf{x})^T W\,\xi(\mathbf{x})$$

where $\xi = (\xi_i),\ i = 1,\dots,m$ is the vector of astrometrical residuals (depending on the orbital parameters $\mathbf{x}$) and W is a square, symmetric, positive-definite $m \times m$ matrix reflecting the *a priori* RMS and correlations of the observation errors.

If such minumum $\mathbf{x}^*$ does exist, we can expand the target function in a neighborhood of $\mathbf{x}^*$:

$$\begin{aligned} Q(\mathbf{x}^*) &= Q(\mathbf{x}^*) + \frac{1}{m}\,(\Delta\mathbf{x})^T\,C\,(\Delta\mathbf{x}) + \dots \\ &= Q(\mathbf{x}^*) + \Delta Q(\mathbf{x})\ , \end{aligned}$$

where $C = B^T W B$ si the *normal* matrix and its inverse is the *covariance* matrix $\Gamma = C^{-1}$. A **Confidence Region** (CR) $Z(\chi)$ is defined by setting an upper limit to the penalty ΔQ:

$$Z(\chi) = \left\{X \mid \Delta Q(X) \le \chi^2/m\right\}\ .$$

If the CR and the residuals are small, then all the higher order terms in the target function are negligible and the confidence region is well approximated by the *confidence ellipsoid* $Z_L(\chi)$ defined by the quadratic inequality

$$Z_L(\chi) = \left\{\mathbf{x}\ :\ \Delta\mathbf{x}^T\,C(\mathbf{x}^*)\,\Delta\mathbf{x} \le \chi^2\right\}\ .$$

This geometrical object is just used for local computations because the hypothesis on the smallness of the residuals is not applicable in general.

However the previous algorithms could fail, when, for example, we have to process a Very Short Arc (VSA), that is a sequence of typically 3 to 5 observations with one hour between the first and the last observation. In most of these cases the arc is too short for a full orbit determination (computation of a LS orbit). When this is the case, the set of observations is called a Too Short Arc (TSA). As it is well known from the theory of preliminary orbit determination, when three observations are used to compute an orbit, the curvature of the arc appears as a divisor in the orbit solution of Gauss' method. The smaller is the curvature, the less accurate is the orbit; taking into account the observational errors, in most cases it turns out to be impossible to apply the usual algorithm, consisting of a preliminary orbit determination by means of Gauss' method followed by a differential correction to obtain a LS orbit. When starting from a TSA, either Gauss' method fails or the differential correction procedure does not converge. For this reason the TSAs are not considered discoveries, but just detections. This does not indicate that the observed object is fictitious, but just that its nature cannot be determined with the information available, that is not possible to discriminate among different classes of object. In [7], the authors faced the problem created by the existence of large databases of TSAs proposing a solution with the introduction of the concept of *attributable*. A TSA is recorded as a set of N observations, which means that a set of points on a straight line is what is actually detected, with deviations from alignment compatible with the random observational error. Thus we can compute the straight line, using a linear regression or something similar. Then a TSA is represented by an attributable, defined in this way:

Definition 1. We call *attributable* a vector

$$\mathcal{A} = (\alpha, \delta, \dot\alpha, \dot\delta) \in [-\pi, \pi) \times (-\pi/2, \pi/2) \times \mathbb{R}^2,$$

representing the angular position and velocity of the body at a time $\bar{t}$ in the selected reference frame.

The attributable could also contain an average apparent magnitude h, if there is at least one measurement of the apparent magnitude available. Note that the information contained in an attributable leaves unknown the topocentric distance ρ (the range) and the radial velocity $\dot{\rho}$ (the range rate) of the object at the reference epoch. If ρ and $\dot{\rho}$ were known, we would have a full description of the asteroid's topocentric position and velocity in polar coordinates $(\alpha, \delta, \dot{\alpha}, \dot{\delta}, \rho, \dot{\rho})$, called also *attributable elements*, which can be easily converted to a Cartesian heliocentric state if the position and velocity of the observer are known.

Given an attributable $\mathcal{A}$, we define the following conditions on ρ and $\dot{\rho}$:

(a) $\mathcal{D}_1 = \{ (\rho, \dot{\rho}) : \mathcal{E}_\oplus \geq 0 \}$ (A is not a satellite of the Earth);

(b) $\mathcal{D}_2 = \{ (\rho, \dot{\rho}) : \rho \geq R_{SI} \}$ (the orbit of A is not controlled by the Earth);

(c) $\mathcal{D}_3 = \{ (\rho, \dot{\rho}) : \mathcal{E}_\odot \leq 0 \}$ (A belongs to the Solar System);

(d) $\mathcal{D}_4 = \{ (\rho, \dot{\rho}) : \rho \geq R_\oplus \}$ (A is outside the Earth).

Definition 2. Given an attributable $\mathcal{A}$, we define as *Admissible Region* (AR) the domain

$$\mathcal{D} = \{ \mathcal{D}_1 \cup \mathcal{D}_2 \} \cap \mathcal{D}_3 \cap \mathcal{D}_4.$$

The AR is a compact set, being the inside of a finite number of closed continuous curves, and it can have at most two connected components (proof in [7]).

Note that in setting the conditions (a)-(d) we have introduced the following assumptions:

- The observer is assumed to be at the geocenter.
- The orbits of asteroids passing close to the Earth are affected by both the attraction of the Sun and that of the Earth; taking into account a complete three-body model would be very complicated. Thus conditions (a) and (b) are approximated, and indeed there are objects in heliocentric orbit experiencing temporary capture as satellites of the Earth, with $\mathcal{E}_\oplus < 0$. However, this can happen only for very low relative velocities Earth-asteroid, and the objects found in these conditions are often artificial.
- When the object is much farther away from the Earth than the Moon, that is $\rho >> 60 R_\oplus$, we should use for $\mu_\oplus$ the ratio between the mass of the Earth-Moon system and the mass of the Sun.
- In computing the radius of the sphere of influence we are neglecting the eccentricity of the orbit of the Earth.

3. **Sampling of the uncertainty region using a swarm of Virtual Asteroids (VAs).** Once the OD procedure is complete (either with a LS orbit and a CR or only with an AR) we would like to explore the uncertainty region (that in both cases is defined as a compact set) sampling it with a finite set of orbits, called **Virtual Asteroids** (VAs). But how to select the VAs? There are essentially two classes of methods: random or Monte Carlo (MC) ones, and geometric sampling methods. The MC methods use the probabilistic interpration ([11]) of the least squares principle, and, when the computational resources are not a problem and the error models are reliable, they are more rigorous and complete with respect to the geometrical methods. Currently, the operative IM systems use the Line Of Variations (LOV) to sample the CR when a LS orbit is available. The LOV is a differentiable curve representing essentially the direction of greater uncertainty, the definition adopted ([8]) is the following.

Definition 3. The LOV is the set of points X such that

$$V_1(\mathbf{x}) || D(\mathbf{x})$$

where V_1 is the unit eigenvector of the normal matrix $C(\mathbf{x}^*)$, computed at the nominal solution, relative to the smallest eigenvalue and $D = -B^T W \xi = -\frac{m}{2} \frac{\partial Q}{\partial \mathbf{x}}^T$.

The equation $V_1(\mathbf{x}) || D(\mathbf{x})$ corresponds to five scalar equations in six unknowns, thus it has generically a smooth one parameter set of solutions, i.e., a differentiable curve. However, we do know an analytic or anyway direct algorithm neither to compute the points of this curve nor to find some natural parameterization (e.g., by the arclength). An algorithm to compute the LOV by continuation from one of its points X is the following. The vector field $F(\mathbf{x}) = k_1(\mathbf{x})\ V_1(\mathbf{x})$, deduced from the weak direction vector field $V_1(\mathbf{x})$, is orthogonal to $H(\mathbf{x})$. A step in the direction of $F(\mathbf{x})$, such as an Euler step of the solution of the differential equation $d\mathbf{x}/d\sigma = F(\mathbf{x})$, that is $\mathbf{x}' = \mathbf{x} + \delta\sigma\ F(\mathbf{x})$, is not providing another point on the LOV, unless the LOV itself is a straight line; this would be true even if the step along the solutions of the differential equation is done with a higher order numerical integration method, such as a Runge-Kutta. However, $\mathbf{x}'$ will be close to another point $\mathbf{x}''$ on the LOV, which can be obtained by applying the constrained differential corrections algorithm ([9]), starting from $\mathbf{x}'$ and iterating until convergence.

If $\mathbf{x}$ was parameterized as $\mathbf{x}(\sigma)$, we can parameterize $\mathbf{x}'' = \mathbf{x}(\sigma + \delta\sigma)$, which is an approximation since the value $\sigma + \delta\sigma$ actually pertains to $\mathbf{x}'$. As an alternative, if we already know the nominal solution $\mathbf{x}^*$ and the corresponding local minimum value of the cost function $Q(\mathbf{x}^*)$, we can compute the χ parameter as a function of the value of the cost function at $\mathbf{x}''$:

$$\chi = \sqrt{m \cdot [Q(\mathbf{x}'') - Q(\mathbf{x}^*)]}\ .$$

In the linear regime, the two definitions are related by $\sigma = \pm\chi$, but this is by no means the case in strongly nonlinear conditions. Thus we can adopt the definition $\sigma_Q = \pm\chi$, where the sign is taken to be the same as that of σ, for an alternate parameterization of the LOV.

In the last year a new method to sample the LOV has been implemented in CLOMON2 ([2], [3]) because, considering that the probability density on the LOV is $p(\sigma) := \frac{1}{\sqrt{2\pi}} e^{-\frac{\sigma^2}{2}}$, the uniform step in σ adopted in the LOV sampling is not optimal; in fact, the probability of each sampling interval would be high around $\sigma = 0$, whereas it becomes too low near the LOV endpoints. Therefore a better choice would be to use a step-size that is inversely proportional to the probability density, small in the points around the nominal solution, and larger towards the points with lower probability. This new sampling procedure is such that the probability of the interval among two consecutive points of the sampling is constant. This means that if $\sigma_{i,i=1,\ldots,N}$ are the sampling nodes, then

$$\mathbb{P}([\sigma_i, \sigma_{i+1}]) := \int_{\sigma_i}^{\sigma_{i+1}} p(\sigma)\, d\sigma$$

does not depend on i. Moreover, to avoid too long intervals around the LOV endpoints, when the interval length exceeds a certain threshold $\Delta\sigma_{max}$ the step-size is set as uniform to this threshold value; this choice is necessary because if the step-size became too large, the last sampling node could fall after the sampling interval endpoints, loosing a portion of the LOV of about the same length of the last step-size.

The LOV method is very useful when the CR is elongated and thin, but this is not the case when the observed arc is very short ($\leq 1^\circ$). When the set of observations of an object covers only a very short arc, the confidence region results to be wide in at least two directions and the LOV is not representative of the entire region: moreover its definition strongly depends upon the coordinates and units used in the OD. In this case, both CLOMON2 and Sentry do not perform very well and a 2-dimensional manifold should be used ([15]), as in the case of imminent impactors that will be described in Section 3.

4. **Propagation of the VAs.** Once a set of VAs have been selected, each orbit is propagated forward to some time in the future, storing all the close approach information obtained during the numerical integration. CLOMON2 propagates VAs until 2100 and maps the linearized uncertainties, represented by the confidence ellipsoids, for all the VAs to the time of each close encounter, allowing an early and quick assessment of whether a potential close encounter could be threatening. The first output of the propagation is a collection of Earth encounters that have been detected for each VA during the time span of interest. If the close encounters set is not empty, the systems perform a sorting of the encounters by date, splitting them into sets that are clustered in time, called *showers*; then, according to the VAs LOV index, they re-sort the showers into contiguous LOV segments, called *trails* (or returns). Each close approach is carefully analysed on the corresponding Target Plane (TP), that is a plane passing through the Earth's center and orthogonal to the unperturbed velocity of the asteroid, i.e., orthogonal to the incoming asymptote of the hyperbola defining the two-body approximation of the trajectory at the time of closest approach ([19], [16]).

5. **Analysis of close approach and detection of Virtual Impactors (VIs).** When there are many points on the TP in a given return it is easy to understand the LOV behaviour because the linear theory is locally applicable. On the contrary, in strong nonlinear cases the LOV has strange behaviours ([15]) and a local analysis is necessary in the neighborhood of each VA. The key point is that the VAs are not just a set of points but they sample a smooth curve, allowing us to interpolate between consecutive sample points. For instance, let us suppose that two consecutive VAs x_i and x_{i+1} have TP trace points y_i and y_{i+1} straddling the Earth impact cross section. If the geometry of the TP trace is simple enough (principle of simplest geometry), an interpolation method provides apoint on the LOV $x_{i+\delta}$ with $0 < \delta < 1$ and such that $y_{i+\delta}$ is inside the Earth impact cross section: then, around $x_{i+\delta}$ there is a VI.

6. **Computation of Impact Probability.** If a VI has been found, by computing the probability density function with a suitable Gaussian approximation centered at $x_{i+\delta}$, it is possible to estimate the probability integral on the impact cross section: this is the impact probability associated with the given VI.

3. IMMINENT IMPACTORS

Small asteroids are expected to strike the Earth every few years and, since such objects are likely to be observed only shortly before the impact, it is important to succeed in an early recognition of hazardous objects. When an object is first observed, the available data are so few that the differential corrections procedure of finding a least-squares orbit could fail and thus they could not permit the determination of a well-constrained six-parameter orbit. Therefore, the short arc OD is a crucial issue and the timing is essential because we are interested in a rapid follow up of the object, to investigate whether could be or not an *imminent impactor*. Three automatic systems were developed recently, SCOUT (at JPL/NASA, [4]), NEORANGER (at University of Helsinki, [13]) and NEOScan (at University of Pisa/SpaceDyS, [14]). We will focus on the last one.

NEOScan consults the NEOCP of the MPC every two minutes, extracting data and running the algorithms based

on the AR (see previous sections), a tool widely used also in the space debris orbit determination ([18]). In particular, the OD algorithm implemented in NEOScan has two choices: it explores a suitable grid in the topocentric range and range-rate space, producing a set of attributable elements, or uses a cobweb sampling of the confidence region to obtain a set of VAs (if a least square orbit does exist). The combination of this two techniques provides a robust short term orbit determination method, which ends with the computation of the Manifold Of Variations (MOV, [17]), a 2-dimensional compact manifold parameterized over the AR. The MOV represents the 2-dimensional analogue of the LOV, thus it is used to sample the set of possible orbits as a starting point for the short term impact monitoring. The goal of NEOScan is to detect all the possible VIs down to a probability level of about 10^{-3}, called completeness level ([3]): the choice of 10^{-3} has been done because we are not interested in lower probability values, given that it is fundamental to avoid unjustified alarms.

Summarizing the algorithm, the steps are the following.

- **Scanning of the NEOCP.** The scan is every two minutes: new and old cases just updated are immediately run, to be confirmed or discarded.
- **Computation and sampling of the AR.** The algorithm provides a two-dimensional representation in the $(\rho, \dot{\rho})$ plane with either a cobweb, if a reliable nominal solution is available, or a double-iteration grid if not. A *reliable nominal solution* is a nominal orbit (i.e., obtained by full differential corrections) with a geodesic curvature signal-to-noise ratio (S/N) χ_{geod} greater than 3.
- **Computation of the MOV and generation of a set of VAs.** Given a subset K of the AR, we define the MOV $\mathcal{M}$ as the set of the points $(\mathcal{A}^*(\boldsymbol{\rho_0}), \boldsymbol{\rho_0})$ in the orbital elements space such that $\boldsymbol{\rho_0} \in K$ and $\mathcal{A}^*(\boldsymbol{\rho_0})$ is the local minimum of the function $Q|_{\boldsymbol{\rho}=\boldsymbol{\rho_0}}$; in addition, the value of the RMS of the residuals is less than a given treshold Σ. In general, the MOV is a two-dimensional manifold, such that the differential of the map from the sampling space to $\mathcal{M}$ has rank 2. In our case, K is the AR, scanned with this first regular semi-logarithmic or uniform grid. For each sample point $\boldsymbol{\rho_0} = (\rho_0, \dot{\rho}_0)$ we fix $\rho = \rho_0$ and $\dot{\rho} = \dot{\rho}_0$ in the target function, and then we search the local minimum $\mathcal{A}^*(\boldsymbol{\rho_0})$ with the same procedure used for classical systematic ranging, that is by means of the *doubly constrained* differential corrections. That procedure works in a similar way as the classical differential correction process, taking into account that two variables are fixed and so working with four-dimensional subspaces: Thus, the normal equation to solve is

$$C_{\mathcal{A}} \Delta\mathcal{A} = D_{\mathcal{A}},$$

where

$$C_{\mathcal{A}} = B_{\mathcal{A}}^T W B_{\mathcal{A}}, \quad D_{\mathcal{A}} = -B_{\mathcal{A}}^T W \boldsymbol{\xi}, \quad B_{\mathcal{A}} = \frac{\partial \boldsymbol{\xi}}{\partial \mathcal{A}}.$$

We indicate as K' the subset of K on which the doubly constrained differential corrections converge; in this way, the sampling of the MOV is performed over K'. For each point $\mathbf{x}$ on the MOV, we also compute a χ value

$$\chi(\mathbf{x}) = \sqrt{m(Q(\mathbf{x}) - Q^*)}, \tag{1}$$

where Q^* is the minimum value of the target function: $Q(\mathbf{x}^*)$ if a reliable nominal solution $\mathbf{x}^*$ exists, or the minimum value of $Q(\mathbf{x})$ over K' otherwise.

- **Propagation and detection of VIs.** The VAs orbits are progated in the future, currently for 30 days, and an analysis on the Modified Target Plane (MTP) is performed in order to find possible impacts. We select as VIs the VAs that, on the MTP, are inside the impact cross section $D_{\oplus}$.
- **IP computation**. If a VI has been found on the MTP, it is associated with an IP computed in this way. We begin assuming that the residuals are a Gaussian random variable $\boldsymbol{\xi}$, with zero mean and covariance $\Gamma_{\boldsymbol{\xi}} = W^{-1}$. Hence the probability density function on the residuals space is

$$\begin{aligned} p_{\boldsymbol{\Xi}}(\boldsymbol{\xi}) = N(\mathbf{0}, \Gamma_{\boldsymbol{\xi}})(\boldsymbol{\xi}) &= \frac{\sqrt{\det W}}{(2\pi)^{m/2}} \exp\left(-\frac{mQ(\boldsymbol{\xi})}{2}\right) \\ &= \frac{\sqrt{\det W}}{(2\pi)^{m/2}} \exp\left(-\frac{1}{2}\boldsymbol{\xi}^T W \boldsymbol{\xi}\right). \end{aligned} \tag{2}$$

The method consists in a rigorous propagation of the density function according to the probability theory without any a priori assumption. The Probability Density Function (PDF) is propagated from the residual space to the orbital elements space (precisely, on the MOV), and then to the sampling space, according to the Gaussian random variable transformation law. The fundamental difference in using this approach instead of the uniform prior distribution (as done in [4]) is that we compute the Jacobian determinant of the transformation and it is not equal to 1. Anyway, the results are similar because, as a matter of fact, the Jacobian determinant is always a number near to unity. To compute the PDF on S (the space of the sampling variables), we start considering the following chain of continuously differentiable maps

$$S \xrightarrow{f_\sigma} \mathbb{R}^+ \times \mathbb{R} \supseteq K' \xrightarrow{f_\mu} \mathrm{x} \supseteq \mathcal{M} \xrightarrow{F|_{\mathcal{M}}} V.$$

where

- K' is the subset of the points of the AR such that the doubly constrained differential corrections give a point on the MOV,
- $\mathcal{M}$ is the MOV,
- $V = F(\mathrm{x})$ is the manifold of the possible residuals, which is a six-dimensional submanifold of $\mathbb{R}^m$,

and we consider the product of the Jacobian determinants. Using the maps f_μ and f_σ, the VI is associated with a subset $\mathcal{V} \subseteq S$ of the sampling space, and hence its probability is given by

$$\mathbb{P}(\mathcal{V}) = \int_{\mathcal{V}} p_{\mathbf{S}}(\mathbf{s})\, d\mathbf{s} =$$

$$\frac{\int_{\mathcal{V}} \exp\left(-\frac{\chi^2(\mathbf{s})}{2}\right) \det M_\mu(\boldsymbol{\rho}(\mathbf{s})) \det M_\sigma(\boldsymbol{\rho}(\mathbf{s}))\, d\mathbf{s}}{\int_{f_\sigma^{-1}(K')} \exp\left(-\frac{\chi^2(\mathbf{s})}{2}\right) \det M_\mu(\boldsymbol{\rho}(\mathbf{s})) \det M_\sigma(\boldsymbol{\rho}(\mathbf{s}))\, d\mathbf{s}}$$

If for a given object we find impacting solutions, we assign to the object an *impact flag*, which is an integer number related to the computation of the impact probability ranging from 0 to 4 and depending on IP and geodetic curvature (see [14] for more details).

- **Computation of object-category score.** Each category of objects (NEO, MBO, DO, SO), given by conditions on the orbital elements, corresponds to a subset $\mathcal{V} \subseteq S$ of the sampling space, and hence the system has the capability to compute the probability of the object to belong to each category making use of the previous formalism.

At the end, the scan is re-scheduled after 2 minutes. The time required to run one target strictly depends on the characteristics of the object, but usually it is between 15 and 20 minutes. When predicting possible imminent impacts, one of the most important requirements to fulfill is to minimize the number of unjustified alarms. It is denoted as *nonsignificant case* an object for which there are less than three observations or the arc length is less than 30 minutes, unless there exists a nominal solution with a geodesic curvature S/N greater than 1. The classification of an object as nonsignificant does not mean that the computation is skipped; all the steps of the algorithm are performed in any case and the score and the impact flag are assigned to the object. Nevertheless, being nonsignificant automatically decreases the priority of the object in case of an alarm. Unfortunately, these techniques are not enough to remove all the spurious cases, they only lower the number. In fact, spurious cases usually occur when the astrometry is either known to be erroneous or noisy, or anyway not reliable. We cannot solve this problem, and we acknowledge that the astrometric error models based on large number statistic are not sufficient to distinguish erroneous and accurate astrometry in a small sample.

3.1. The latest impactor: 2018LA

Last year NEOScan had the opportunity to be real time tested on a real case of an imminent impactor: the asteroid 2018 LA. This object, known as ZLAF9B2 prior to being designated, was a small Apollo-type NEA that impacted Earth's atmosphere at roughly 16:44 UTC (18:44 local time) on 2 June 2018 over Botswana, near South Africa border, at the altitude of about $h = 50$ km. The asteroid produced an explosion with an intensity of about 1 kiloton, which suggests an estimated size for the asteroid of 3 to 5 meters in diameter, and it was discovered only 8 hours prior the impact by Richard Kowalski at the Mount Lemmon Survey. The object approached the Earth with a relative velocity of approximately 17 km/s from the night side: due to its size and high entry velocity, it could not have been spotted before it was very close to the Earth, and it could only be detected on its final plunge to Earth. Indeed, when it was first detected, the asteroid was nearly as far away as the Moon's orbit and appeared as a streak in the series of time-exposure images taken by the Catalina telescope.

The first observations data were immediately submitted to the MPC and published on the NEOCP. In the following hours additional observations were made and, according to the system results, as the number of the observations was increasing, it became extremely probable that the object would have collided with the Earth.

During the follow up, 4 tracklets of observations were obtained: the first one was of 3 observations, the second and the third of 11 and 12 observations, respectively, and the last of 14 observations. Table 1 shows the outcomes of the software while observations were flowing in. Table 1 shows how the IP increased as new observations were added. By using the last tracklet, consisting of 14 observations, the system estimated that the impact would have certainly occurred ($IP = 100\%$), and thus, according also to the arc quality, gave the impact flag the maximum value.

# of observations	Impact Probability
3	0.08%
11	5.1%
12	38.3%
14	100%

Table 1. Number of observations and corresponding values of IP, impact flag and the score.

Table 2 displays additional information for each tracklet: details upon the corresponding arcs and results of the software by means of the number of grid and MOV points and, among them, the *impacting points*. We recall that κ is the geodesic curvature and $\dot{\eta}$ is the along-track acceleration, while *Overall* indicates their chi^2-value χ^2_c. The item *Arc Type* in Table 2 indicates an integer number N defined as follows. An observed arc is an *Arc of Type N* if it can be split into exactly N disjoint TSAs in such a way that each couple of TSAs consecutive in time, if joined, would show a significant curvature. The computation of the arc type value depends upon the method by which the observed arcs are to be split into TSAs; the values in Table 2 have been computed by using the algorithm discussed in [10].

We now report the results obtained by NEOScan for each one of these observed arcs, thus revealing how the awareness of an impacting object increased as the observations were flowing in ([1]).

# Obs.	Time span (h)	Arc Type	Significance of curvature κ	Significance of curvature $\dot{\eta}$	Significance of curvature Overall	# of points	MOV points	Impacting points
3	0.38	1	0.22	1.78	1.82	10000	5304	166
11	1.42	2	-0.42	61.21	61.39	10000	634	168
12	1.42	2	-1.91	63.47	63.56	10000	584	177
14	3.78	3	187.67	-369.07	409.56	10000	8811	8811

Table 2. For each tracklet, number of observations, arc data and specific results.

First observed arc: 3 observations The first three observations were made in the early morning of Saturday 2 June 2018, and covered a time span of 22.8 minutes; the absolute magnitude of the body was estimated between a minimum value $H_{min} = 31.29$ and a maximum value $H_{max} = 34.39$, thus indicating a small object. This batch of observations was immediately submitted to the MPC NEOCP, where the object was temporarily denoted as ZLAF9B2; the NEOScan run started at 09:04 UTC and ended at 09:18 UTC. We refer to Table 1 and Table 2 for the main results and arc data. The observed arc was an arc of type 1, since it had a non significant curvature. In this case, only the double grid sampling of the AR could be adopted because the observational data were too poor to compute a nominal solution; in particular, the software computed a uniform densified grid in $log_{10}(\rho)$ for the AR.

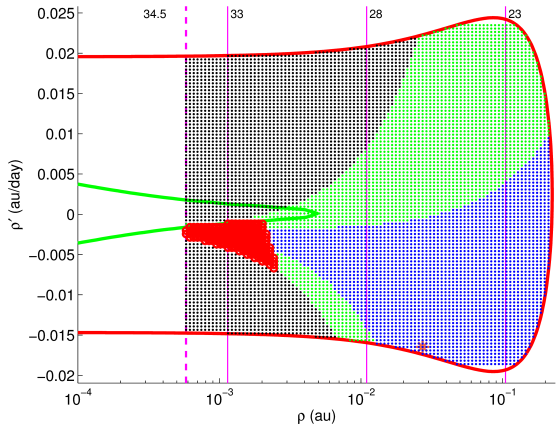

Figure 1. Grid sample of the AR in the $(\rho, \dot{\rho})$ space for the first 3 observations of 2018 LA.

Figure 1 shows the uniform AR grid sampling obtained with NEOScan for the three observations tracklet:

- the red solid line represents the level curve of the heliocentric energy equal to $-k^2/(2a_{max})$, namely, the outer boundary of the AR;
- the green dashed line shows where the geocentric energy is equal to 0, also taking into account the condition about the radius of the Earth sphere of influence;
- the magenta dashed line (which is parallel to the $\dot{\rho}$ axis) represents the shooting star limit condition;
- the magenta solid lines (which are parallel to the $\dot{\rho}$ axis) represent different values of the absolute magnitude;
- the dots are indicated in blue if $\chi(\mathbf{x}) \leq 2$, green if $2 < \chi(\mathbf{x}) \leq 5$ and black if $\chi(\mathbf{x}) > 5$;
- the points corresponding to a VI are represented with red circles.

The grid consists of 10000 points while, as displayed in Table 2, the corresponding MOV consists of 5304 points (the coloured points in Figure 1); among them, there are 166 impacting points (the red circles in Figure 1), which lead to an impact probability value $IP = 0.08\%$. Therefore, due to this IP value, the system assigned impact flag 1 to the object. Furthermore, with such a grid sampling, the score of the object to be classified as a NEA was 100%. In Figure 2 it is easy to see that there are some

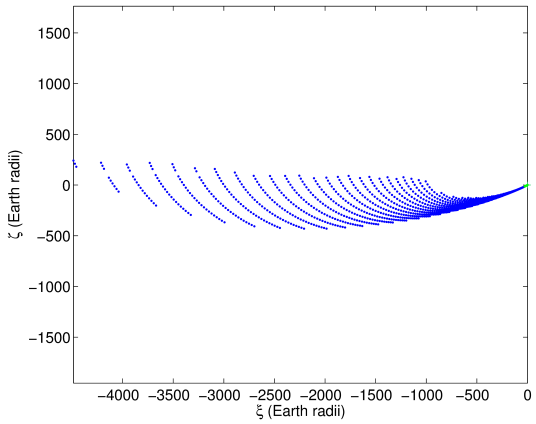

Figure 2. Projection on the MTP of the VAs obtained with the first 3 observations of 2018 LA.

blue points leading to an impact, and thus corresponding to a VI.

With these first three observations available only, the object was claimed as *nonsignificant* because the arc length was $\Delta t = 22.8$ min, that is less than the minimum established (30 minutes) in order to avoid unjustified alarms. Nonetheless, the impact flag value 1 and NEA score

100% produced an alert for the observers, and a follow up of the object was immediately started.

Second observed arc: 11 observations Within two hours, additional observations of the object ZLAF9B2 were provided, giving an amount of 11 total observations; the arc covered a longer time span, $\Delta t = 85.2$ min, and then the object was no longer classified as a nonsignificant case. The observed arc resulted an arc of type 2, with a significant curvature; moreover, the value of the geodesic curvature S/N was $\chi_{geod} < 3$.

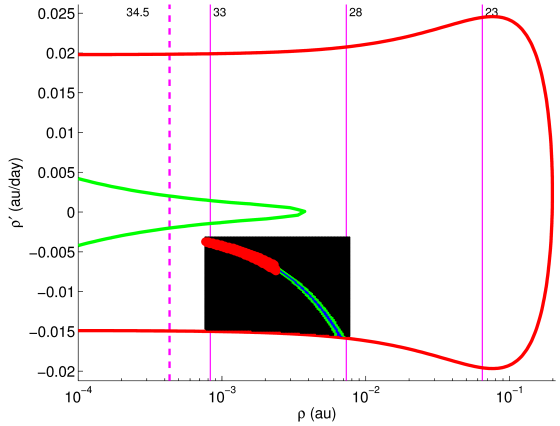

Figure 3. Grid sample of the $(\rho, \dot{\rho})$ space for 11 observations of 2018 LA.

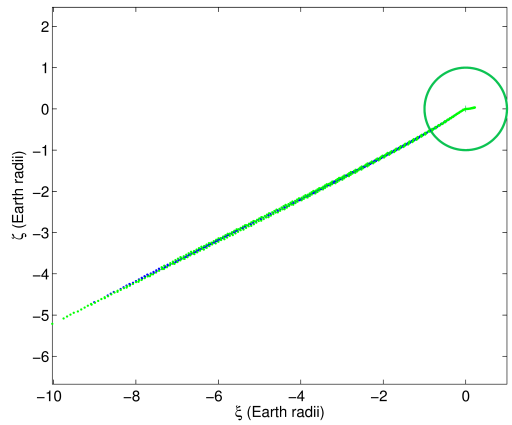

Figure 4. Projection on the MTP of the VAs obtained for 11 observations of 2018 LA.

The NEOScan software run started at 11:41 UTC and ended at 11:57 UTC, giving results as displayed in Table 1 and Table 2. Again, a reliable nominal solution could not be obtained and thus the software had to apply the double grid sampling of the AR, computing a uniform densified grid in $log_{10}(\rho)$. With such a grid sampling, the score of the object to be classified as a NEA was 100%. Figure 3 shows the uniform AR grid sampling obtained for this eleven observations tracklet; the used colour scheme is the usual. Again, the grid consists of 10000 points while, as displayed in Table 2, the corresponding MOV consists of 634 points only; among them, there are 168 impacting points, which lead to an impact probability value $IP = 5.1\%$. Hence, according to this IP value and to the fact that $\chi_{geod} < 3$, the system assigned impact flag 3 to the object, thus increasing its priority in the follow up activities. Figure 4 represents the projection on the MTP of the VAs. The colours of the points indicate their χ-value, according to the usual colour code, while the dark green circle centerd in $(0, 0)$ is the Earth cross section. Figure 4 clearly shows a number of projected MOV points inside the Earth cross section, which form a VI and thus correspond to the red circles in Figure 3.

Third observed arc: 12 observations In a matter of minutes, one additional observation was provided; thus, with a total of 12 observations, the observed arc still covered a time span $\Delta t = 85.2$ min, and was an arc of type 2, with a significant curvature. Indeed, its curvature is very slightly different from the one of the tracklet with 11 observations. NEOScan run started at 14:10 UTC and ended at 14:26 UTC. Again, since it still could not be obtained a reliable nominal solution, the software had to apply the double grid sampling of the AR, and computed a uniform densified grid in $log_{10}(\rho)$ consisting of 10000 points; with such a grid sampling, the score of the object to be classified as a NEA was 100%.

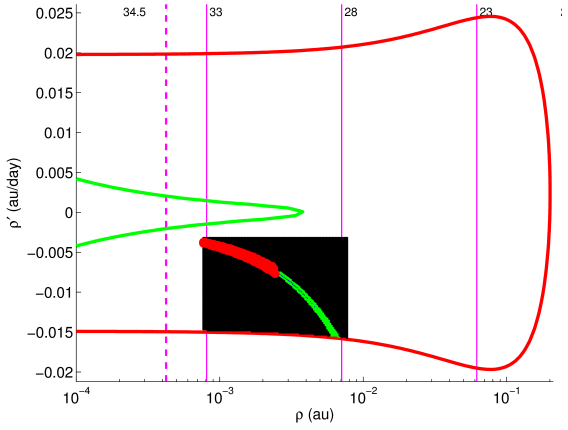

Figure 5. Grid sample of the $(\rho, \dot{\rho})$ space for 12 observations of 2018 LA.

Figure 5 shows the uniform AR grid sampling obtained for this tracklet with 12 observations. According to Table 2, with a single additional observation the software was able to compute a MOV consisting of 584 points, where the impacting points were 177, thus decreasing the number of VAs while increasing the number of impacting points. As a consequence, the impact probability increased significantly, reaching the value $IP = 38.3\%$. Figure 6 represents the projection on the MTP of the VAs, using the usual colour scheme and a dark green circle centerd in $(0, 0)$ representing the Earth cross section; it clearly shows a number of projected MOV points inside

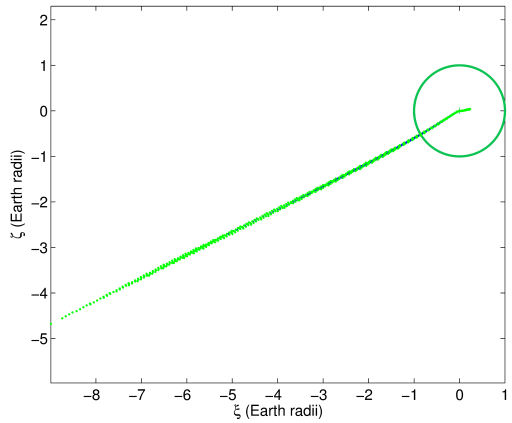

Figure 6. Projection on the MTP of the VAs obtained for 12 observations of 2018 LA.

the Earth cross section, thus leading to an impact. These orbits form a VI and correspond to the red circles in Figure 3. Again the system assigned impact flag 3 to the object, since the observed arc still had $\chi_{geod} < 3$, and at that point it was clear that every single additional observation would have been critical to ascertain whether the impact would occur or not.

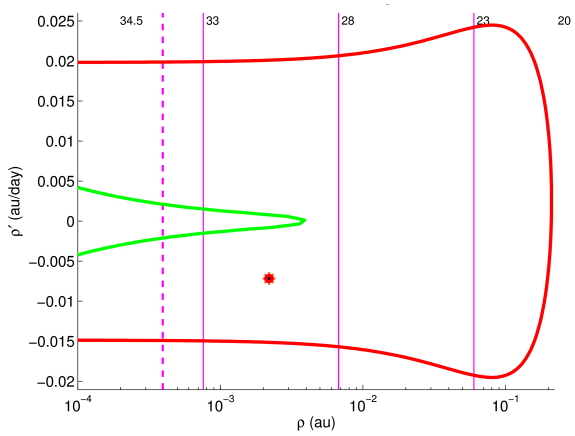

Figure 7. The AR in the $(\rho, \dot{\rho})$ space for 14 observations of 2018 LA.

Fourth observed arc: 14 observations In about two hours, two additional observations of ZLAF9B2 were obtained, giving an amount of 14 total observations and determining a tracklet that covered a time span $\Delta t = 226.8$ min. This tracklet was an arc of type 3, and allowed the system to compute a reliable nominal solution $\mathbf{x}^*$ with $RMS = 0.571$. Using the new observations, the absolute magnitude of the body was estimated more precisely, between $H_{min} = 30.55$ and $H_{max} = 30.59$, thus the small object resulted slightly bigger than was expected initially with only 3 observations. NEOScan run started at 14:13 UTC and ended at 14:40 UTC; since a reliable nominal solution was available, the software performed a cobweb sampling of the AR in a neighborhood of $\mathbf{x}^*$.

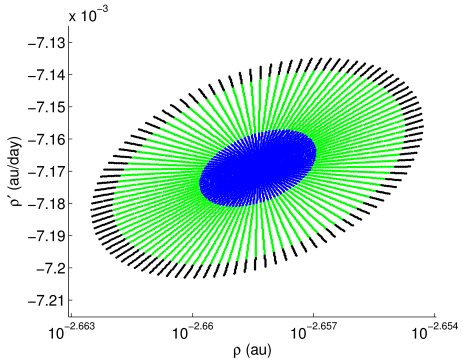

Figure 8. Cobweb sampling of the $(\rho, \dot{\rho})$ space for 14 observations of 2018 LA.

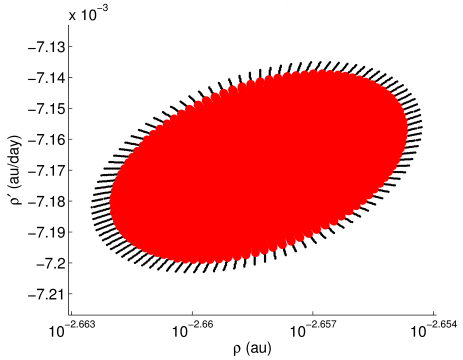

Figure 9. Cobweb sampling of the $(\rho, \dot{\rho})$ space for 14 observations of 2018 LA. Here the impacting points are shown.

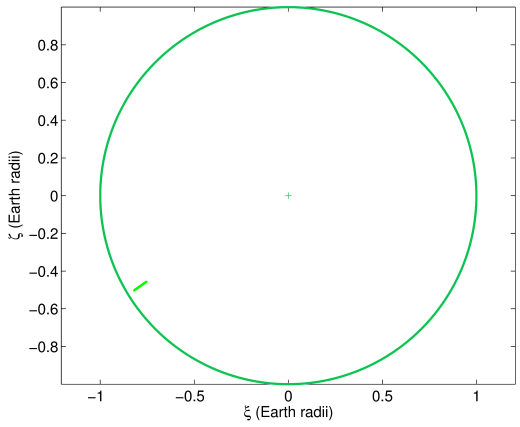

Figure 10. Projection on the MTP of the VAs obtained for 14 observations of 2018 LA.

In Figure 7 is shown the AR obtained with this tracklet of 14 observations; around the point denoted with the orange star (that is the orbit with the minimum χ^2 value) there are the points of the cobweb sampling, which is very small with respect to the whole AR and thus it is not visible in this graphic. Figure 8 and Figure 9 provide a zoomed representation of the cobweb sampling inside the AR. Figure 8 shows the cobweb sampling by denoting

points with colours indicating their χ-value; on the other hand, Figure 9 shows the cobweb sampling indicating the impacting orbits with red circles. The sample consists of 10000 points while the MOV consists of 8811 points, which are all impacting orbits, as one can see in Table 2; indeed, the MOV is represented by green and blue dots (that is, the orbits having $\chi \leq 5$), and by comparing Figure 8 and Figure 9 it is easy to see that all the MOV points are denoted with the red circles, that is they are all impacting orbits. Therefore, NEOScan computed an impact probability value $IP = 100\%$, and then, obviously, assigned impact flag 4 to the object. Figure 10 represents the projection on the MTP of the VAs; it shows that all the projected MOV points are inside the Earth cross section, thus pointing out that the impact would certainly occur. At that point it was necessary to rapidly predict the impact corridor ([2]), to outline possible impact locations in such a way to allow the organisation of quick security measures.

4. FUTURE OF IMPACT MONITORING

At the moment there are two types of automatic systems dealing with IM of NEOs:

(1) those for already designated orbits, like CLOMON2 and Sentry, and

(2) those for the detections of imminent impactors (SCOUT, NEORange, NEOScan).

Systems of class (1) use data from MPEC, and a geometrical sampling of the CR with the LOV, while those of class (2) scan the NEOCP and use systematic ranging methods and/or geometric sampling with a 2-dimensional manifold.

The born of this two classes of systems has been essentially dictated by the history of searching for NEOs, by the grow of observational facilities and by the amount of data available. When CLOMON2 and Sentry started their activities the scientific and public communities were interested in big objects that could have caused global damage, while, at the moment, the attention has moved to small objects and meteorites. Probably, the differentiation in this two classes are due also to the rules of the MPC, or better, how the automatic systems catch the data from it. In this processes there could be a flaw, in the sense that there are objects, with a very well-defined orbit, remaining on the NEOCP, and, on the contrary, there exist designated objects with a great uncertainty. Thus, there are a certain number of cases that are not properly processed: object with a very well defined orbit should be processed like ordinary cases using, for example, LOV methods, while designated objects would deserve a treatment using a different sampling of the CR.

What we propose and what we will try to develop in the next years is an unified system that, starting from NEOCP data of an object, could decide the type of orbit and what is the more corrected algorithm of OD to extract as much information as possible.

The starting step should use the NEOScan algorithms to give a first insight to the observational data and to understand, using the *score* of the detection, the type of orbit. The score is the probability that an object belongs to the classes listed below:

- **NEO**: Near-Earth Object, an object with perihelion distance $q < 1.3\,AU$;
- **MBO**: Main Belt Object, an object belonging either to the Main Belt or to the Jupiter Trojans. In particular, it has to fulfill the conditions

  $$\begin{cases} 1.7\,AU < a < 4.5\,AU \\ e < 0.4 \end{cases} \vee \begin{cases} 4.5\,AU < a < 5.5\,AU \\ e < 0.3 \end{cases}$$

  where a is the semimajor axis (in AU) and e is the eccentricity;
- **DO**: Distant Object, characterized by $q > 28\,AU$ (for instance, a Kuiper Belt Object);
- **SO**: Scattered Object, not belonging to any of the previous classes.

In case of a NEO probability greater than some thresold, the algorithms for searching VIs should start. The choice of the more convenient algorithm should be based on some facts and quantities:

- type of observational arc;
- geodetic curvature;
- presence or not of a reliable LS orbit.

Knowing the previous input, the system must be able to decide:

a) the way to sample the uncertainty region (AR or CR);

b) the duration of propagation;

c) how to detect potential impactors after the propagation and the projection on the TP of an encounter.

Concerning a), a possible improvement is the use of a Monte Carlo (MC) sampling of the CR, when a nominal solution exists. MC method start from a given probability distribution of initial conditions and propagated forward in time while recording the number of impacts. This kind of method has the advantage of making no simplifying assumptions on how the orbital uncertainties are mapped into the future. However, MC method is a very computationally expensive technique because it requires propagating a large number of VAs, typically of the order of

the inverse of the target probability resolution. However, due to increase in the speed of processors, new MC-type methods are being studied ([12]) in order to replace geometrical sampling. A new automatic system, like what we have in mind, should have the capability of use both a geometrical sampling or MC method and above all understand when to use one and when the other.

5. CONCLUSIONS

In the last twenty years there has been a huge progress in the problem of assessing the asteroid impact hazard. But, as pointed out in [5], the story is not finished, the research in this field must go on. Due to LSST and GAIA, there will be a significant increase in the amount and quality of data and, both the mathematical algorithms and the processing strategies, should be improved. In this paper we presented the state of art of IM systems, higlighting the features of classical IM (LOV geometrical sampling) and discussing a new generation system, NEOScan, treating imminent impactors. We showed also the analysis of a real case, 2018LA. At the end we proposed some possible future developments in the field of IM, and the idea of developing a unique automatic system capable of summarize the features of CLOMON2 and NEOScan in itself.

ACKNOWLEDGMENTS

This conference paper is dedicated to Andrea Milani Comparetti (1948-2018) who was, without a shadow of a doubt, the founding father of impact monitoring and the first scientist to develop an automatic system for asteroid hazard. We should have written this work together and he would certainly has enlightened me with new ideas that were never lacking. Unfortunately fate has decided otherwise, depriving us of his brilliant intuition and his ideas never banal. But I am sure that what he has done will inspire all future scientists who will dedicate to planetary protection.

REFERENCES

1. Bertolucci A., (2018). Impact Monitoring of Near-Earth Objects: old algorithms and new challenges, *Master Thesis, University of Pisa*
2. Del Vigna A., (2018) On Impact Monitoring of Near-Earth Asteroids, *PhD thesis, University of Pisa*
3. Del Vigna A., et al., (2019). Completeness of Impact Monitoring, *Icarus*, **321**, pp. 347-360
4. Farnocchia D., et al., (2015). Systematic ranging and late warning asteroid impacts, *Icarus*, **258**, pp. 18-27
5. Farnocchia D., (2016). Impact hazard monitoring: theory and implementation, *Proc. of the IAU Symposium 318*, CUP, pp. 221-230
6. Marsden B.G, Williams G.V., (1998). The NEO confirmation page, *Planetary Space Science*, **46**(2), pp. 299-302
7. Milani A., et al., (2004). Orbit determination with very short arcs. I admissible regions, *Celestial Mechanics and Dynamical Astronomy*, **90**(1), pp. 59-87
8. Milani A., et al., (2005). Multiple solutions for asteroid orbits: computational procedure and applications, *Astronomy & Astrophysics*, **431**, pp. 729-746
9. Milani A., et al., (2005). Nonlinear impact monitoring: line of variation searches for impactors, *Icarus*, **173**, pp. 362-384
10. Milani A., et al., (2007). New Definition of Discovery for Solar System Objects, *Earth, Moon and Planets*, **100**(1-2)
11. Milani A., Gronchi G. F., (2010). Theory of Orbit Determination, Cambridge University Press
12. Roa J., Farnocchia D., (2018). Multilayer clustered sampling technique (MLCS) for Near-Earth Asteroid Impact Hazard Assessment, AAS 19-260
13. Solin O., Granvik M., (2018). Monitoring near-Earth-object discoveries for imminent impactors, *Astronomy & Astrophysics*, **616**
14. Spoto F., et al., (2018). Short arc orbit determination and imminent impactors in the Gaia era, *Astronomy & Astrophysics*, **614**
15. Tommei G., (2005). Nonlinear impact monitoring: 2-dimensional sampling, *Proc. of the IAU Colloquium 197*, CUP, pp. 259-264
16. Tommei G., (2006). Canonical elements for Öpik theory, *Celestial Mechanics and Dynamical Astronomy*, **94**, pp. 173-195
17. Tommei G., (2006). Impact Monitoring of Near Earth Objects: theoretical and computational results, *Ph.D. Thesis in Mathematics*, University of Pisa
18. Tommei G., (2007). Orbit determination of space debris: admissible regions, *Celestial Mechanics and Dynamical Astronomy*, **97**(4), pp. 289-304
19. Valsecchi G. B., et al., (2003). Resonant returns to close approaches: Analytical theory, *Astronomy & Astrophysics*, **408**, pp. 1179-1196
20. Veres P., et al., (2018). Unconfirmed Near-Earth Objects, *The Astronomical Journal*, **156**(5)
21. Virtanen J., et al., (2001). Statistical Ranging of Asteroid Orbits, *Icarus*, **154**